



**Title:** Whitelight SPR and Measurement of Kinetics for Indolicidin, IL4 and IL8  
**Subject:** Master Thesis  
**Projectperiod:** 1st of september 2010 - 22nd of september 2011

**Author:**

Per Francek

**Supervisor:** Leonid Gurevich

**Number of copies:** 7  
**Report page count:** 28  
**Appendix page count:** 0  
**[Total page count:]** 31  
**Ended:** 31st of May 2010

*The content of this report is freely available, but publication, partly or in full, may only happen with proper citation.*

# Contents

<b>1</b>	<b>Abbrevitions</b>	<b>3</b>
1.1	abbreviations . . . . .	3
<b>2</b>	<b>Introduction</b>	<b>4</b>
2.1	Introduction . . . . .	4
2.1.1	Antimicrobial Peptides . . . . .	4
2.1.2	Indolicidin . . . . .	5
2.2	Surface Plasmon Resonance . . . . .	5
2.2.1	Excitation of Surface Plasmons by Light . . . . .	8
2.2.2	DNA Immobilization on Gold Chips . . . . .	8
2.2.3	Binding kinetics . . . . .	8
2.2.4	Fluid Dynamics . . . . .	10
<b>3</b>	<b>Materials and Methods</b>	<b>11</b>
3.1	Materials and Methods . . . . .	11
3.1.1	Protocol for Immobilization of Biotinylated DNA on SPR Sensorchip HX 200m and SPR Sensorchip HC 200m . . . . .	11
3.1.2	IL8 binding assay . . . . .	11
3.1.3	IL4 binding assay . . . . .	12
3.1.4	immobilization of thiolated DNA on Bare Gold Chips . . . . .	12
3.1.5	Indolicin Binding Assay With Chambers Connected in Serial . . . . .	12
3.1.6	Indolicidin Binding Assay With Chambers connected in parallel . . . . .	12
3.1.7	Calibration of waste tube length . . . . .	12
3.1.8	Data Treatment . . . . .	13
3.1.9	White Light SPR . . . . .	13
<b>4</b>	<b>Results</b>	<b>15</b>
4.1	Results . . . . .	15
4.1.1	IL4 Binding Assay . . . . .	15
4.1.2	IL8 Binding assay . . . . .	15
4.1.3	Calibration of Waste Tube Length . . . . .	15
4.1.4	Indolicidin Binding Assay With Chambers Connected in Parallel . . . . .	17
4.1.5	White Light SPR . . . . .	18
<b>5</b>	<b>Discussion</b>	<b>23</b>
5.1	Discussion . . . . .	23
<b>6</b>	<b>Conclusion</b>	<b>28</b>
6.1	Conclusion . . . . .	28

# Abbreviations

---

## 1.1 abbreviations

HEPES = (4 - (2 - *hydroxyethyl*) - 1 - *piperazineethanesulfonicacid*)

NaOH/NaCl = 2M NaCl + 10mM NaOH in DI H<sub>2</sub>O

EDC = 1 - *ethyl* - 3 - (3 - *dimethylaminopropyl*)*carbodiimide*)

NHS = 1 - *Hydroxy* - 2,5 - *pyrrolidinedione*

TRIS = *tris*(*hydroxymethyl*)*aminomethane*

IL4 = Indolicidine with tryptophan 4 retained and remaining substituted by leucines

IL8 = Indolicidine with tryptophan 8 retained and remaining substituted by leucines

DNA = Deoxyribonucleic acid

## 2.1 Introduction

Drug resistant strains of pathogens are emerging at an alarming rate world wide [1] and it is commonly believed that there are two prime reasons for this. Low concentrations of antibiotics are commonly used in animal feed to prevent disease and enhance growth [2]. While this is advantageous for the farmers, the low concentration of antibiotics allow pathogens to develop resistance to the antibiotics. Strains of Salmonella were found in ground beef and 80% of them were shown to be resistant to at least one type of antibiotic [2] and as such antibiotic resistant strains of pathogens are known to cross over from animals to humans [3][4]. The other reason is the use of antibiotics in treatment of diseases and infections in humans [5]. As a result drug resistance in pathogens is on the rise and alternatives are needed.

### 2.1.1 Antimicrobial Peptides

Promising candidates are AntiMicrobial Peptides (AMPs). They can offer a broad activity range and a wide range of possible modifications should resistances to AMPs develop. Antimicrobial peptides are a part of the innate immune system found in eukaryotes. They serve to defend the host against pathogens while the body's adaptive immune system is activated if this is needed. While the primary target of AMPs is bacterial membranes, they are known to target both bacteria [6], virus [7], fungi [8] and even tumors [9].

The method of action is known for some AMPs adopting an amphipathic  $\alpha$ -helical conformation while attached to membranes, while others are still debated. Proposed models include the carpet model [10], the barrel stave model and the toroidal porre model [11].

#### The Carpet Model

In the carpet model, the AMP attach parallel to the membrane via electrostatic interactions. Due to the electrostatic interactions the peptides cannot reorient and the interaction the hydrophobic residues of the peptide and the polar head groups of the membrane causes strain in the membrane. Once a certain surface concentration of peptide is reached the membrane becomes sufficiently unstable and disintegrate [12] [13].

#### The Barrel Stave Model

In the barrel stave model the peptides also attach to the surface. As the the concentration increases the peptides may form oligomers and start to migrate into the membrane, the peptides oligomers inside the membrane may then recruit additional peptides to increase the pore size. The activity here is mainly driven by hydrophobic interactions and is therefore not limited to negatively charged membranes. [13] [12]

#### The Toroidal Porre model

In this model a pore is also formed however the toroidal porre model is different from the barrel stave model in that the pore formed also contains hydrophilic headgroups in its interior so that the water core of the pore is exposed to hydrophilic residues from the peptide and hydrophilic headgroups from the membrane lipids.

### 2.1.2 Indolicidin

Indolicidin is a cationic antimicrobial peptide with the sequence ILPWKWPWWPWRamide containing the highest amount of Trp ever seen at 39% [6]. Indolicidin exhibits a broad antimicrobial activity, but unfortunately for the potential of its direct medicinal use it also shows cytotoxic activity against Human T lymphocytes [14]. Several analogs of indolicidin have been produced [15][16][14], in attempts to lower or limit the cytotoxicity while retaining as much antimicrobial activity as possible or at times enhancing it.

In 2010 an Indolicidin analog named omiganan was the most promising AMP based drug candidate showing activity against acne and catheter related infections [16].

While indolicidin is toxic to mammalian cells, two derivatives, named IL4 and IL8 are not while they retain much of the anti microbial activity of indolicidin. The sequence of the two analogs are the indolicidin with tryptophans at position 4 and 8 respectively retained and all other Trp residues exchanged with leucines.

Indolicidin is thought to act by binding to phospholipids [17] however its mode of action is not completely determined [18].

Indolicidin has been shown to bind to DNA and its sequence preference has been determined along with rate constants and equilibrium constants. [19] This has been done with Surface Plasmon Resonance which is a powerful tool for characterizing binding events.

## 2.2 Surface Plasmon Resonance

Maxwell's equations in the absence of external sources are given by [20]:

$$\nabla \times \mathbf{E} = -\frac{\partial \mathbf{B}}{\partial t} \quad (2.1)$$

$$\nabla \cdot \mathbf{D} = 0 \quad (2.2)$$

$$\nabla \times \mathbf{H} = \frac{\partial \mathbf{D}}{\partial t} \quad (2.3)$$

$$\nabla \cdot \mathbf{B} = 0 \quad (2.4)$$

With  $\mathbf{E}$  being the electric field,  $\mathbf{B}$  being the magnetic flux density,  $\mathbf{H}$  being the magnetic field and  $\mathbf{D}$  being the dielectric displacement field.

The solution to the Maxwell's equations in the case of a plane wave is given by [20][21]:

$$E = E_0 e^{i(\mathbf{k} \cdot \mathbf{r} - t\omega)} \quad (2.5)$$

$$B = B_0 e^{i(\mathbf{k} \cdot \mathbf{r} - t\omega)} \quad (2.6)$$

Surface plasmons are excited by the electric field normal to the surface and therefore if surface plasmons are to be excited by an electromagnetic wave there must be an electric field component normal to the surface. Defining the coordinates as the surface in the xy plane, the z plane perpendicular to the surface and the incident beam propagating along the x direction as sketched in figure 2.1 the previously mentioned requirement becomes  $E_z \neq 0$ . The requirement is not fulfilled for s-polarized light and therefore only p-polarized light can excite surface plasmons[20][22]. Written for p-polarized light and divided into components equation 2.6 becomes[22].

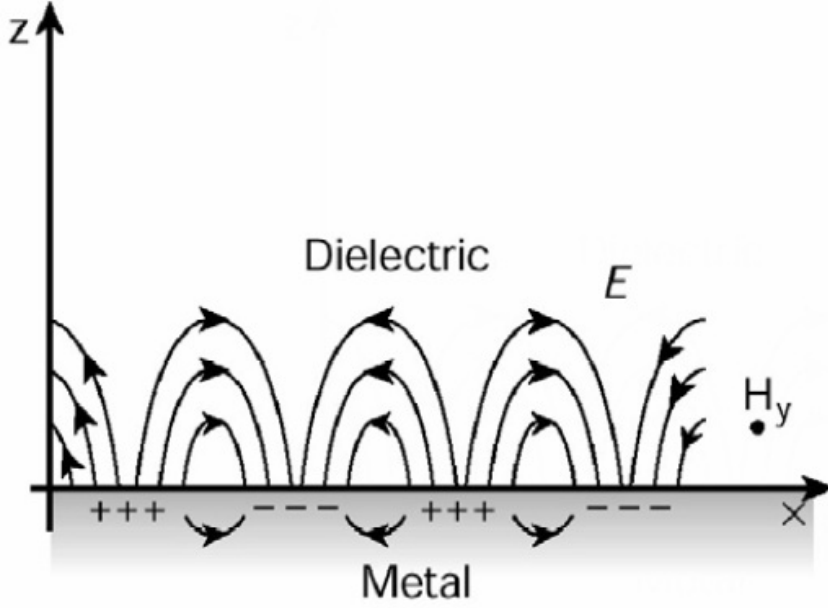


Figure 2.1: Illustration of Surface plasmons propagating along the x axis on the interface between a metal and a dielectric, with the plane of incidence being the xz plane. [22]

For  $z > 0$

$$\mathbf{E} = (E_{xd}, 0, E_{zd})e^{i(k_{xd}x+k_{zd}z-t\omega)} \quad (2.7)$$

$$\mathbf{B} = (0, B_{yd}, 0)e^{i(k_{xd}x+k_{zd}z-t\omega)} \quad (2.8)$$

For  $z < 0$

$$\mathbf{E} = (E_{xm}, 0, E_{zm})e^{i(k_{xm}x-k_{zm}z-t\omega)} \quad (2.9)$$

$$\mathbf{B} = (0, B_{ym}, 0)e^{i(k_{xm}x-k_{zm}z-t\omega)} \quad (2.10)$$

With d and m denoting dielectric and metal respectively. Inserting equations 2.7 and 2.10 into equation 2.3 yields two separate equations; one for the dielectric:

$$\nabla \times \mathbf{H}_d = \frac{\partial \mathbf{D}_d}{\partial t}$$

$$H_{yd}(-\hat{x}k_{zd} + \hat{z}k_{xd}) = -\epsilon\epsilon_0(E_{xd} + E_{zd})$$

Divided into components

$$-H_{yd}\hat{x}k_{zd} = -\epsilon_d\epsilon_0 E_{xd} \quad (2.11)$$

$$H_{yd}\hat{z}k_{xd} = -\epsilon_d\epsilon_0 E_{zd} \quad (2.12)$$

And one for the metal:

$$\nabla \times \mathbf{H}_m = \frac{\partial \mathbf{D}_m}{\partial t}$$

$$H_{ym}(-\hat{x}k_{zm} + \hat{z}k_{xm}) = -\epsilon\epsilon_0(E_{xm} + E_{zm})$$

Divided into components

$$-H_{ym}\hat{x}k_{zm} = -\epsilon_m\epsilon_0 E_{xm} \quad (2.13)$$

$$H_{ym}\hat{z}k_{zm} = -\epsilon_m\epsilon_0 E_{zm} \quad (2.14)$$

as  $\mathbf{D} = \epsilon\epsilon_0\mathbf{E}$ .

Under the assumption that both the dielectric and the metal are linear, homogeneous, local and isotropic the electric field component parallel and the dielectric displacement field component perpendicular to the interface are continuous across the interface [21] as is the y component of the magnetic field[22], i.e.  $\mathbf{E}_{xd} = \mathbf{E}_{xm}$ ,  $\mathbf{D}_{zd} = \mathbf{D}_{zm}$  and  $\mathbf{H}_{yd} = \mathbf{H}_{ym}$ . Using the z component of equations 2.11, 2.12, 2.13 and 2.14 along with the continuities of  $H_y$ ,  $D_z$  it can be seen that the component of the wavevector parallel to the interface is continuous across the interface:

$$k_{xd} = k_{xm} = k_x \quad (2.15)$$

Using the x component of equations 2.11, 2.12, 2.13 and 2.14 and the continuities of  $E_x$  and  $H_y$  it can be seen that:

$$\frac{k_{zd}}{\epsilon_d} = -\frac{k_{zm}}{\epsilon_m} \quad (2.16)$$

This shows that surface plasmons can only exist on an interface between two materials having dielectric constants of opposite signs. Under the previously mentioned assumption that the mediums are linear, local, isotropic and homogeneous the magnetude of  $\mathbf{k}$  is given by:

$$k_i = \sqrt{k_{xi}^2 + k_{yi}^2 + k_{zi}^2} = \frac{\omega}{c}\sqrt{\epsilon_i} \quad (2.17)$$

The index i denoting either dielectric or metal.  $\mathbf{k}_{xi} = \mathbf{k}_x$  being continuous and  $\mathbf{k}_y = 0$  this leaves:

$$k_d^2 = k_x^2 + k_{zd}^2 = \left(\frac{\omega}{c}\right)^2 \epsilon_d \quad (2.18)$$

$$k_m^2 = k_x^2 + k_{zm}^2 = \left(\frac{\omega}{c}\right)^2 \epsilon_m \quad (2.19)$$

These two equations along with equation 2.16 yield the dispersion relation for the x component of the surface plasmons [22]:

$$k_x = \frac{\omega}{c} \sqrt{\frac{\epsilon_d\epsilon_m}{\epsilon_d + \epsilon_m}} \quad (2.20)$$

### 2.2.1 Excitation of Surface Plasmons by Light

In order to excite surface plasmons by light it is required that  $k_x$  for the surface plasmon and  $k_x$  for the incident light, now termed  $k_{xl}$ , match at a given frequency, this can never happen by lighting the dielectric side directly as:

$$k_{xl} = \frac{\omega}{c} \sqrt{\epsilon_d} \sin(\theta) < \frac{\omega}{c} \sqrt{\frac{\epsilon_d \epsilon_m}{\epsilon_d + \epsilon_m}} = k_x \quad (2.21)$$

$k_{xl}$  approaches  $k_x$  asymptotically and they never intersect [22]. However, surface plasmons can be achieved using attenuated total reflection (ATR) and the resulting evanescent wave from the other side if a prism with a relative electric permittivity  $\epsilon_p > \epsilon_d$  is used. The surface plasmons are affected by the presence of the prism and the finite thickness of the metal layer and this introduces a correction in the dispersion of the surface plasmon [23]:

$$k_{sp} = \frac{\omega}{c} \sqrt{\frac{\epsilon_d \epsilon_m}{\epsilon_d + \epsilon_m}} + \Delta k_{sp} \quad (2.22)$$

The excitation condition then becomes:

$$\frac{\omega}{c} \sqrt{\frac{\epsilon_d \epsilon_m}{\epsilon_d + \epsilon_m}} + \Delta k_{sp} = \frac{\omega}{c} \sqrt{\epsilon_p} \sin(\theta) \quad (2.23)$$

This becomes possible as  $\epsilon_p > \epsilon_d$  and therefore the dispersions no longer asymptotically approach and can now intersect.

### 2.2.2 DNA Immobilization on Gold Chips

Several methods have been developed for immobilization of various bio molecules on gold surfaces for the purpose of conducting SPR experiments [23]. Direct covalent attachment is desired for it's robustness as it is important for the immobilized layer to be so stable that dissociation of the layer is negligible. This is necessary for a global fit of binding curves obtained by SPR to make sense and also in order to insure that the experiment can be completed before the immobilized layer is gone.

Thiolated DNA is reported to form ordered mixed monolayers with mercaptohexanol. It achieves a low density of immobilized DNA which is ideal for eliminating or reducing mass transport effects. The mercaptohexanol also prevents nonspecific binding of DNA. [24] In some cases covalent attachment may not be desirable as the molecule intended for capture may be unstable under the conditions required for the chemical reactions involved in the covalent immobilization [23]. A very widespread method is capture by streptavidin [23] due to the very strong but non covalent binding to biotin [25]. It requires that the molecule intended for capture is biotinylated in order to take advantage of the high affinity. Streptavidin itself can be immobilized by standar amine coupling it has been shown to be a useful method for determining binding kinetics and affinities for a DNA binding compound [24].

### 2.2.3 Binding kinetics

#### Equilibrium Constant Determination

The equilibrium of a binding reaction is described by the Langmuir model [26]:



Where P is the DNA and X is the peptide and  $K_A$  is the equilibrium association constant which is equal to:

$$K_A = \frac{[X][P]}{[XP]} \quad (2.25)$$

where the brackets denote concentration. The fraction of DNA binding sites bound by a peptide is then given by the concentration of peptide bound to DNA divided by the total number of DNA binding sites:

$$\theta = \frac{[XP]}{[XP + P]} = \frac{K_A[X][P]}{[P] + K_A[X][P]} = \frac{K_A[X]}{1 + K_A[X]} \quad (2.26)$$

The response in relation to bound concentration is a linear function [27]. Therefore  $\theta$  can be substituted:

$$\theta = \frac{R_{eq}}{R_{max}} \quad (2.27)$$

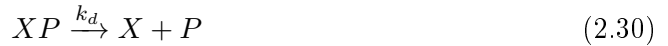
With this substituted into the Langmuir model  $K_a$  can be calculated from a series of equilibrium measurements:

$$\begin{aligned} \frac{R_{eq}}{R_{max}} &= \frac{K_A[X]}{1 + K_A[X]} = \frac{1}{\frac{1}{K_A[X]} + 1} \\ &\Downarrow \\ \frac{R_{eq}}{R_{max}} + \frac{R_{eq}}{K_A[X]R_{max}} &= 1 \\ &\Downarrow \\ \frac{R_{eq}}{[X]} &= R_{eq}K_A + R_{max}K_A \end{aligned} \quad (2.28)$$

A plot of  $R_{eq}$  divided by  $[X]$  against  $R_{eq}$  can then be made from a series of equilibrium measurements resulting in a line with slope of  $-K_A$  and  $R_{max}$  can then be calculated.

### Binding Rate Constants

The binding of indolicidin, IL4 and IL8 to DNA is assumed to follow a 1:1 binding model so that[28]:



Where  $k_a$  is the association rate constant and  $k_d$  is the dissociation rate constant. The concentration of free peptide times the concentration of free DNA multiplied by the association rate constant characterizes the rate at which peptide binds to DNA, the amount of bound peptide times the dissociation rate constant characterizes the rate at which the bound peptide dissociates from the DNA, so that the total change in in bound peptide concentration is:

$$\frac{d[XP]}{dt} = k_a[X]([P] - [XP]) - k_d[XP] \quad (2.32)$$

This can be rewritten because the response is directly proportionate to the amount of bound peptide [29]:

$$\frac{dR}{dt} = k_a[X](R_{max} - R) - k_dR \quad (2.33)$$

Which is solved by [29] [30] [31]:

$$R(t) = \frac{k_a[X]R_{max}}{k_a[X] + k_d} \left(1 - e^{-t(k_a[X] + k_d)}\right) \quad (2.34)$$

The dissociation phase starts when buffer, free of peptide, is injected into the reaction chambers, i.e.  $[X] = 0$ . Inserting this into equation 2.32 yields:

$$\frac{dR(t)}{dt} = -k_d R(t + t_0) \quad (2.35)$$

Where  $t_0$  is the time at which the dissociation phase started. This is then solved by exponential decay [31]:

$$R(t) = R(t_0)e^{-k_d(t-t_0)} \quad (2.36)$$

Equations 2.34 and 2.36 can then be fitted to the obtained SPR curves to determine  $k_a$  and  $k_d$ . It is recommended to use nonlinear least-squares fitting [32] as linearization of the differential equations also linearize any errors present making them harder to interpret [30].

### 2.2.4 Fluid Dynamics

#### Serial Flow

The setup typically used in the SR7000DC is a serial connection of the chambers as shown in figure 2.2: The sample is injected into the reaction chamber, then exits the reaction chamber and enters the reference chamber.

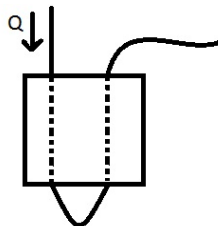


Figure 2.2: Schematic representation of serial injection setup

Taylor dispersion is the result of combined diffusion and convection resulting in an effect that results in a broadening of the sample as it flows through the tubing. In itself Taylor dispersion will dilute the sample at the interface between sample and running buffer and, if the effect is large, create a non-uniform concentration profile [33] which will result in significant error in the SPR curve. This carries over to fitting of the SPR data introducing these errors into the kinetics data obtained from the experiment.

Another issue emerges when serial connecting the chambers. Taylor dispersion is a time dependant phenomenon [33] and the sample has extra time to disperse while it is in the tube connecting the two chambers, leading to a difference in the concentration profiles in the two chambers respectively.

This is not the only problem: Each time the sample enters or exits a chamber it goes from one type of tube cross section to another, creating a mixing effect in the concentration profile smearing it even further. as the sample enters the first chamber this happens once but while the sample is passing from one chamber to the other it happens two additional times creating additional mixing in the sample.

## 3.1 Materials and Methods

Acetic acid was obtained from Merck KGaA. EDC, EDTA, Ethanolamine, HEPES, MES, NHS, immersion oil, Streptavidin, TRIS, Mercaptohexanol, DTT and Tween 20 were obtained from SIGMA-ALDRICH A/S. Bare gold SPR Sensorchips and SPR sensorchip HX 200m and SPR Sensorchip HC 200m were purchased from Xantec. Thiolated DNA with the sequence: CAT ATA TAT ATC CCC CAT ATA TAT ATG and Biotinylated DNA with the sequence: 5'biotEG-CATATATATATATCCCCATATATATATG were obtained from Eurofins MWG Operon.

The solutions used in the experiments can be seen in table 3.1, all solutions were filter degassed prior to use.

Polarizer and pinhole for the whitelight setup was purchased from Thorlabs. Lenses were purchased from Edmund Optics UK, Ltd.

Table 3.1: Solutions used in the experiments

Name of Solution	Component 1	Component 2	Component 3	Component 4	pH value
HEPES Buffer	DI Water	150mM NaCl	3.4mM EDTA	0.05% Tween 20	7.4
TE Buffer	DI Water	10mM Tris	1mM EDTA		8
TE high salt buffer	1M NaCl	10mM Tris	1mM EDTA		8
NaOH/NaCl	2M NaCl	10mM NaOH			9.3

### 3.1.1 Protocol for Immobilization of Biotinylated DNA on SPR Sensorchip HX 200m and SPR Sensorchip HC 200m

The SPR sensorchip HX 200m or HC 200m chip was mounted in the SR7000 and 5mM Sodium acetate pH 5.0 buffer was used as running buffer at a flowrate of 50 $\mu$ L/min the system was wired to have flow through both chambers. 2M NaCl and 150mM NaOH in H<sub>2</sub>O solution was injected for 5 minutes, after this running buffer was used again. This was repeated three times. A solution of 0.5M NHS and 0.5M EDC was injected for 6 minutes, then the flow was stopped and acetic acid was injected for 2 minutes. Streptavidin in HEPES buffer with a concentration of 1mg/ml was subsequently injected for 20minutes. After this HEPES buffer was injected for 15minutes followed by ethanolamine for another 15minutes. The chamber was then rewired to only allowed flow through the chamber to the right chamber hereafter termed the reaction chamber. Biotinylated DNA is then injected for 20minute and HEPES is then injected for 4minutes. The chambers are then rewired to allow flow through both chambers again.

### 3.1.2 IL8 binding assay

For these experiments the chip prepared in section 3.1.1 was used.

At the beginning of each day of these experiments three four minute injections of NaOH/NaCl were done at a flowrate of 40 $\mu$ L/min.

Injections of concentrations 0.2 $\mu$ M, 0.5 $\mu$ M, 1 $\mu$ M, 2 $\mu$ M and 5 $\mu$ M respectively of Indolicidine8 were then performed after eachother with a NaOH/NaCl injection after each in-

dolicinde injection these were performed at a flowrate of  $40\mu\text{L}/\text{min}$  for four minutes. Injections of  $0.2\mu\text{M}$ ,  $0.5\mu\text{M}$ ,  $1\mu\text{M}$ ,  $2\mu\text{M}$ ,  $5\mu\text{M}$  and  $10\mu\text{M}$  were performed in the same way at a flowrate of  $20\mu\text{L}/\text{min}$  for twenty, forty and fifty minutes each. After each injection of either NaOH/NaCl or IL8 the injection loop was cleaned with DI water.

### 3.1.3 IL4 binding assay

For these experiments the chip prepared in section 3.1.1 was used.

Before each set of experiments three four minute injections of NaOH/NaCl were done at a flowrate of  $40\mu\text{L}/\text{min}$ .

Injections of concentrations  $0.2\mu\text{M}$ ,  $0.5\mu\text{M}$ ,  $1\mu\text{M}$ ,  $2\mu\text{M}$  and  $5\mu\text{M}$  respectively of Indolicidine4 were then performed after each other with a NaOH/NaCl injection after each indolicinde injection these were performed at a flowrate of  $40\mu\text{L}/\text{min}$ . After each injection of either NaOH/NaCl or IL8 the injection loop was cleaned with DI water.

### 3.1.4 immobilization of thiolated DNA on Bare Gold Chips

Bare gold chips were first exposed to UV light for 15minutes and then bathed in ethanol for 20minutes. The chip was then mounted in the SR7000. The Running buffer used was TE buffer with  $1\text{MNaCl}$ . Thiolated DNA was deprotected using  $100\text{mMDTT}$  in  $10\text{mM}$  TE pH 8 for 30min. Afterwards the sample was purified by running the sample through two Illustra NAP-5 columns (GE Healthcare, Little Chalfont, UK). A known volume of DNA solution was taken out and diluted to determine OD for the purpose of determining concentration. The DNA then injected through the right chamber only at an initial flowrate of  $30\mu\text{L}/\text{Min}$  which was then lowered to  $4\mu\text{L}/\text{min}$  once the SPR signal changed due to the sample entering the chamber. The thiolated DNA was injected for 3 hours. The chambers were then rewired to allow flow through both chambers and Mercaptohexanol was injected in both chambers for 30 minutes at a flowrate of  $3\mu\text{L}/\text{min}$ . The chambers were then cleaned

### 3.1.5 Indolicin Binding Assay With Chambers Connected in Serial

Chambers were connected in serial and a prepared bare gold chip was used. Indolicidin samples of concentrations 0.5, 1, 2 and  $5\mu\text{M}$  respectively dissolved in HEPES buffer were injected at a flowrate of  $30\mu\text{L}/\text{min}$  for four minutes after which they were allowed time to dissociate. After each injection of Indolicidin an injection of NaCl and NaOH in DI water was performed.

### 3.1.6 Indolicidin Binding Assay With Chambers connected in parallel

Chambers were connected in parallel and a prepared bare gold chip was used. Indolicidin samples of concentrations 1, 2, 5 and  $10\mu\text{M}$  respectively dissolved in HEPES buffer were injected at a flowrate of  $30\mu\text{L}/\text{min}$  for four minutes after which they were allowed time to dissociate.

### 3.1.7 Calibration of waste tube length

The waste tubes after the SPR flowcell chambers were used to modify the flow resistance of the system to allow for the most uniform flow possible. Solutions of Ethylene Glycol in water was injected at flowspeeds 10, 20, 30 and  $40\mu\text{L}/\text{min}$  respectively. Curves were obtained using the Reichert SPR V.4.0.17 software and loaded in Open Office Calc for further treatment. The time from injection till 5% of the max response was calculated

for each chamber for each injection by approximating a line between the two data points neighbouring 5% of the max response and thus approximating a more correct time value for 5% of the max response. The time taken from injection till reaching the stream splitter was then subtracted to obtain the time taken from separation of the flows till the samples enter the respective chambers. The relationship between the two times was then obtained. The relationship between the times was then used as the relationship between the flow resistances after flow separation. This was used to determine the fraction of one tube to be cut off for the flow resistances to be the same. The calculated tube length was then cut off.

### 3.1.8 Data Treatment

After assays were performed, curves from both chambers were selected for each sample injection using Reichert SPR V.4.0.17 software. The data was then loaded into Scrubber2 version 2b from biologic software. In Scrubber2 the concentrations of each injection was entered and all of the curves were zeroed, by selecting a small portion of baseline from before each injection and setting the two chamber responses to both average to zero in that region. After this the curve from the right chamber was aligned to that of the left chamber so that the resulting referenced curve was as smooth as possible and so that the general features of the original curves were matched as closely as possible to each other. Then the injections of concentration 0 were used as a double reference by subtracting the response from these injection from the other injections with a concentration different from 0. Then in the ‘‘kinetics’’ tab the injection start and end times were specified and  $k_d$  or  $k_d$  and  $k_a$  or alternatively  $k_d$ ,  $k_a$  and  $k_m$  are attempted fit to the obtained binding curves.

### 3.1.9 White Light SPR

A holder for a BK7 prism was designed to mimic the specifications of the flowcell used in the SR7000DC. The flowcell from the SR7000DC was then used for the experiment. The setup in order from light source to spectrometer was: Halogen lamp lightsource, lens lens to focus the beam, pinhole, lens to colimate the beam, polarizer, prism with flowcell and gold chip, lens and fiber optic cable into the photo spectrometer as shown in figure 3.1. The flowcell from the SR7000DC was used in one experiment and a newly designed flowcell with one large fluidic chamber was used in the others.

Measurements were done after initially obtaining a dark spectrum by covering the input of

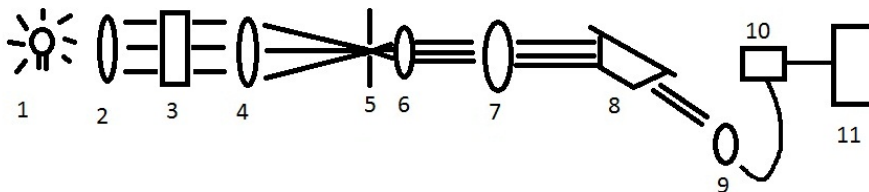


Figure 3.1: *Diagram of the whitelight SPR setup. 1: 100W, 12V Halogen lamp, 2: Colimator lens, 3: IR filter (DI water), 4:focusing lens, 5: pinhole, 6:colimating lens, 7: Polarizer, 8: gold chip, 9: lens and optics cable, 10: JAZ Photo spectrometer, 11: Personal Computer*

the spectrometer and pressing the dark measurement button in the Spectra Suite software. DI water was injected into the flowcell and a reference spectrum was taken by setting the polarizer to allow only s-polarized light to pass through and pressing the reference spectrum button in the Spetra Suite software. Then the Spectra Suite software was set to reflection mode and the polarizer was set to allow p-polarized light to pass through. The

## Materials and Methods

---

spectrum was then examined for the SPR feature position. Then air was injected into the flowcell, and the change in position of the SPR feature was observed.

# Results

---

## 4.1 Results

### 4.1.1 IL4 Binding Assay

SPR sensorgrams of IL4 and hairpin DNA were obtained by injecting varying concentrations of IL4 onto a hydrogel chip with immobilized DNA. It was treated as described in section 3.1.8 to obtain binding curves. The curves with the best fit are presented in figure 4.1.

The curves show the expected dependency of concentration versus signal response with the  $2\mu M$  injection reaching the highest response, the  $1\mu M$  injection reaching the second highest response and the  $0.2\mu M$  injection reaching the lowest response. An injection of  $0.5\mu M$  was also performed, but it did not yield a proper binding curve.

Obtained kinetic values are  $k_a = 3.615$   $k_d = 8.756 * 10^{-3}$   $R_{max} = 3.193 * 10^5$  and  $K_d = 2.42228mM$  with residual standard deviations 13.636, 7.937 and 4.392 for  $2\mu M$ ,  $1\mu M$  and  $0.2\mu M$  respectively. Only in the injection of  $0.2\mu M$  does the bound IL4 appear to have dissociated after 5 minutes.

### 4.1.2 IL8 Binding assay

SPR sensorgrams of IL8 and DNA were obtained as described in section 3.1.2 and treated as described in section 3.1.8 to obtain binding curves. The curves with the best fit are presented in figure 4.2.

Obtained kinetic values are  $k_a = 55.83$ ,  $k_d = 0.005707$   $K_d = 102.224\mu M$  with R max values of 2930.2, 4023.5, 3814.3 and 1916.1 for  $2\mu M$ ,  $0.2\mu M$ ,  $0.5\mu M$  and  $1\mu M$  respectively and Residual standard deviations of 3.456, 2.542, 2.691 and 2.665 for  $2\mu M$ ,  $0.2\mu M$ ,  $0.5\mu M$  and  $1\mu M$  respectively.

### 4.1.3 Calibration of Waste Tube Length

As the data obtained with the serial connection of reference and measurement chamber show significant difference in the injection response between reference and measurement chambers (see figure 4.3) a set of measurements with the chambers connected in serial was performed. To ensure identical flow through the chambers with this configuration the hydraulic resistance of the chambers should be the same. Fine tuning of the hydraulic resistance was done by adjusting the length of the tube between the chamber the waste bottles. The tubelength calibration was performed by injecting ethylene glycol and measuring the time from injection till response.

The tubing for the flow cell was set up as shown in figure 5.1. Ethylene Glycol was injected and the time it took to reach the chamber from the flow split was determined as described in section 3.1.7. Times and ratio of the times  $\frac{t}{7}$  can be seen in table 4.1.

The times increase as flowrate decreases as expected. The difference between the times for left and right increases as the flowrate increases which is also to be expected. Other injections were also made however one of the chambers appeared to have had its flow cut off or severely slowed during these and manual intervention was required for this to be rectified, therefore this injection has not been included. Unexpectedly the ratio of the times changes as the flowrate changes. As a consequence of this the waste receptacle was

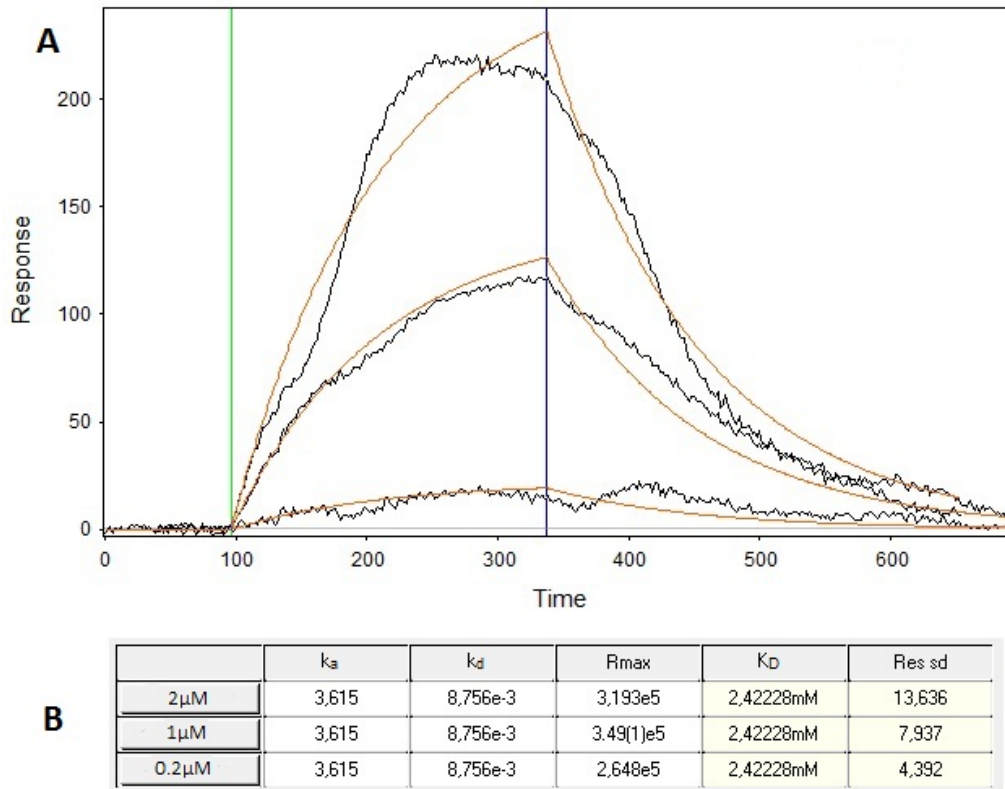


Figure 4.1: (A) SPR sensorgram obtained from four minute injection of  $2\mu M$ ,  $1\mu M$  and  $0.2\mu M$  IL4 injection at  $40\mu L/min$  the  $2\mu M$  injection is the one reaching the highest response, the  $1\mu M$  injection is the one reaching the second highest response and the  $0.2\mu M$  injection has the lowest response. Curves are treated as described in section 3.1.8. The two vertical lines mark the beginning and ending of the injections. The flow chambers are connecte in serial.  $\mu RIU$  on the y-axis and seconds on the x-axis. (B) The binding kinetics obtained from the sensorgram,  $[k_a] = M^{-1}s^{-1}$ ,  $[k_d] = s^{-1}$ ,  $[R_{max}] = \mu RIU$  and  $[K_d] = mM$

moved to allow the waste tubes to bend as little as possible. identical measurements were performed again and results are shown in figure 4.2.

The times increase as flowrate decreases as expected. Two different measurements at  $20\mu L/min$  gave results with a difference of several seconds signifying an unstable over-all flowrate this is strange as the pump is set to deliver a certain flowrate, not a certain pressure. There is a difference between the ratios of  $t_r$  to  $t_l$  but it does not appear to correlate to the flowrate in any discernable fashion, this is not ideal, but small errors can be expected. The same is the case with  $\Delta t$  however here a correlation was expected;  $\Delta t$  was supposed to increase as flowrate is lowered. It should also be noted that the ratios of  $t_r$  to  $t_l$  are generally larger than one, whereas they were generally lower in table 4.1. While the wastetubes were positioned to bend the least possible  $\Delta t$  was always positive although not entirely stable. Therefore it was decided that the right waste tube was to be shortened. The ratio closest to 1 was 1.025, correponding to 2.5%, the right waste tube was shortened by 60% of this amount in order to err on the side of caution.

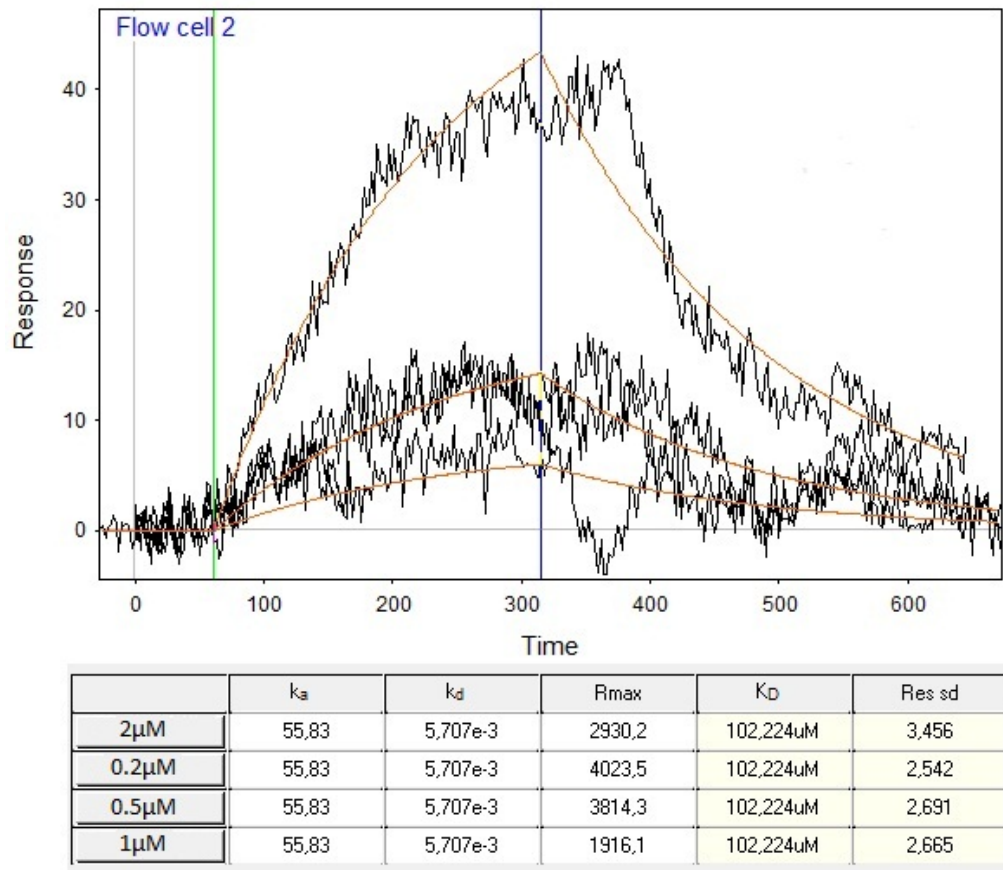


Figure 4.2: (A) SPR sensorgram obtained from four minute injection of  $2\mu M$ ,  $1\mu M$ ,  $0.5\mu M$  and  $0.2\mu M$  IL8 injection at  $40\mu L/min$  the  $2\mu M$  injection is the one reaching the highest response, the  $1\mu M$  and the  $0.5\mu M$  injections are on top of each other as second and third highest response and the  $0.2\mu M$  injection has the lowest response. Curves are treated as described in section 3.1.8. The two vertical lines mark the beginning and ending of the injections. The flow chambers are connected in serial.  $\mu RUI$  on the y-axis and seconds on the x-axis. (B) The binding kinetics obtained from the sensorgram,  $[k_a] = M^{-1}s^{-1}$ ,  $[k_d] = s^{-1}$ ,  $[R_{max}] = \mu RUI$  and  $[K_d] = mM$

#### 4.1.4 Indolicidin Binding Assay With Chambers Connected in Parallel

SPR sensorgrams of indolicidin and hairpin DNA were obtained as described in section 3.1.6 and treated as described in section 3.1.8 to obtain binding curves. The curves with the best fit are presented in figure 4.4.

The injections made into a flowchamber set up with parallel injections was expected to yield less artifacts. this was not the case. The artifacts present have almost the same magnitude as the highest signal present, making the curve fittings terrible.

The correlation between signal strength versus concentration was as expected. The  $10\mu M$  injections reached the highest response, the  $5\mu M$  injections reached the second highest response, the  $2\mu M$  injections had the second lowest responses and the  $1\mu M$  injection had the lowest response.

It was necessary to allow scrubber to use different values of  $R_{max}$  for different concentra-

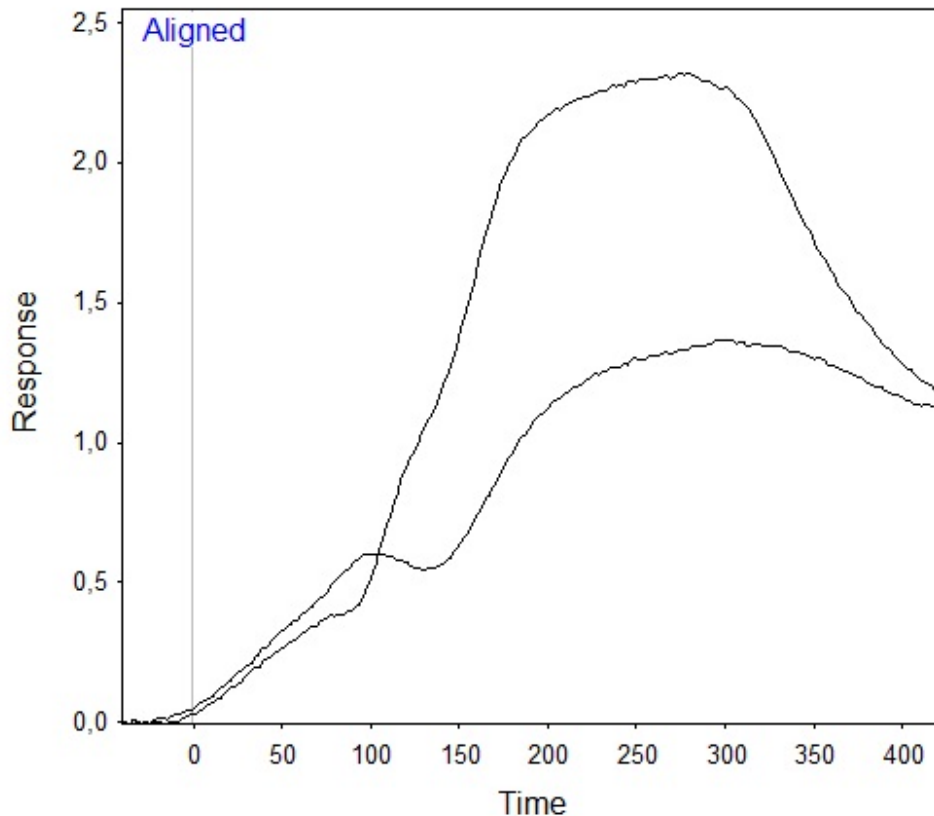


Figure 4.3: *Left and right chamber responses to  $5\mu M$  IL4 injection. A typical sensorgram with significant differences in the injection responses.*

tions This was necessary in order to get kinetics values that were not of the form  $0(xe^n)$  which translates to  $0 \pm x(e^n)$ . The best curve fitting was obtained using a model that takes mass transport into account. Obtained kinetics values are:  $k_m = 55272.5$   $k_a = 824 * 10^7$ ,  $k_d = 775.7$   $K_d = 9.41478\mu M$  with R max values of 2930.2, 4023.5, 3814.3 and 1916.1 for  $2\mu M, 0.2\mu M, 0.5\mu M$  and  $1\mu M$  respectively and Residual standard deviations of 3.456, 2.542, 2.691 and 2.665 for  $2\mu M, 0.2\mu M, 0.5\mu M$  and  $1\mu M$  respectively.

#### 4.1.5 White Light SPR

The optical equipment was set up as described in section 3.1.9. A bare gold chip was mounted on the BK7 prism and the flow cell was attached on top and an intensity profile of reflection versus wavelength was obtained as described in section 3.1.9. Using equation 2.23 along with the assumption that  $\Delta K_{sp} \approx 0$  and material constants from [34] it was determined that to achieve a resonance wavelength between 575nm and 600nm an angle of between 77.28 degrees and 81.56 degrees was needed. The angle was adjusted so it was between these angles. The resonance wavelength was around 700nm as shown in figure 4.5 The focused beam of light hitting the gold chip was larger than the fluidic chambers and a resonance wavelength lower than 700nm could not be achieved. Therefore it was theorized that the position of the dip was a result of the relatively small contact area of water compared to that of air and rubber from the flowcell. For this reason a new flow chamber was designed to have the liquid in the chamber cover the majority of the chip.

Table 4.1: Time taken for the sample to reach the chambers at various flow rates and ratio of times right/left.  $t_r$  is time to reach right chamber from the flow is split.  $t_l$  is time taken to reach left chamber after the flow is split.

Flowrate	$t_l$ [s]	$t_r$ [s]	Ratio r/l	$\Delta t$ (right-left)[s]
$40\mu Lmin^{-1}$	159.981	160.051	1.000	0.070
$30\mu Lmin^{-1}$	235.883	235.624	0.998	-0.25
$20\mu Lmin^{-1}$	289.765	284.453	0.981	-5.311

Table 4.2: Time taken for the sample to reach the chambers at various flow rates and ratio of times right/left.  $t_r$  is time to reach right chamber from the flow is split.  $t_l$  is time taken to reach left chamber after the flow is split.

Flowrate	$t_l$ [s]	$t_r$ [s]	Ratio r/l	$\Delta t$ (right-left)[s]
$40\mu Lmin^{-1}$	75.106	81.818	1.089	6.711
$30\mu Lmin^{-1}$	104.372	107.305	1.028	2.932
$20\mu Lmin^{-1}$	150.013	157.891	1.052	7.878
$20\mu Lmin^{-1}$	147.635	151.329	1.025	3.694
$10\mu Lmin^{-1}$	264.756	272.501	1.029	7.745

The same setup was used again with the exception of the flow cell which was replaced with the new flowcell with a larger flow chamber. a reflectance curve vs wavelength was recorded in the same way as in the earlier experiments and the dip was observed to be very close to 600nm as can be seen in figure 4.6 A second order polynomial was fitted to the SPR dip as shown in figure 4.6 and the minimum was determined from this polynomial to be 619.74nm. The fit is reasonable with  $r^2 = 0.9842$ . The value of 620.75nm is close to the expected value.

In order to confirm that the minimum observed was indeed caused by surface plasmons, 99.99% Ethanol was injected along with 5%, 10%, 20% and 50% ethylene glycol to observe the shift in resonance wavelength. The reflectance graphs can be seen in figure 4.7.

It can be seen that that injecting ethanol shifted the resonance wavelength towards a higher wavelength as expected. injection of 5% ethylene glycol shifted the wavelength to a lower wavelength compared to water. injections of higher concentrations of ethylene glycol shifted the resonance wavelength further to a higher wavelength, the resonance wavelengths can be seen in table 4.3.

Table 4.3: Refractive index and resonance wavelength of the solutions injected into the flow chamber

Solution	Refractive index (780 nm)	Resonant wavelength	
Water	1.33	620.75nm	1.089
Ethanol	1.35	649.6939nm	1.028
5% Ethylene glycol	1,3328785458	607.7434nm	
10% Ethylene glycol	1,3374605815	614.9774nm	
20% Ethylene glycol	1,3469385977	629.1818nm	
50% Ethylene glycol	1,3768322025	700.6538nm	

0=620.75 etoh=649.6939 5102050

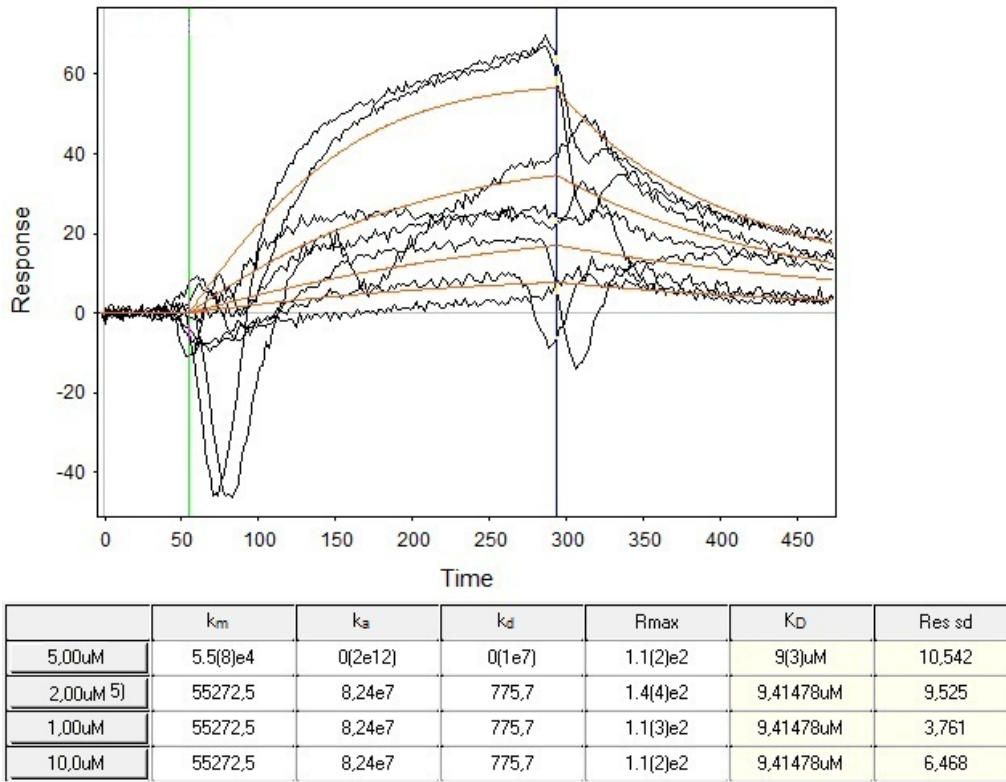


Figure 4.4: (A) SPR sensorgram obtained from four minute injection of  $2\mu M$ ,  $1\mu M$ ,  $10\mu M$  and  $5\mu M$  indolicidin at  $40\mu L/min$ . There are two of each injection. The  $10\mu M$  injection is the one reaching the highest response, the  $5\mu M$  injection is the one reaching the second highest response, the  $2\mu M$  injections have the second lowest responses and the  $1\mu M$  injection reaches the lowest response. Curves are treated as described in section 3.1.8. The two vertical lines mark the beginning and ending of the injections. The chambers are connected in parallel.  $\mu RIU$  on the y-axis and seconds on the x-axis. (B) The binding kinetics obtained from the sensorgram,  $[k_a] = M^{-1}s^{-1}$ ,  $[k_d] = s^{-1}$ ,  $[R_{max}] = \mu RIU$  and  $[K_d] = mM$

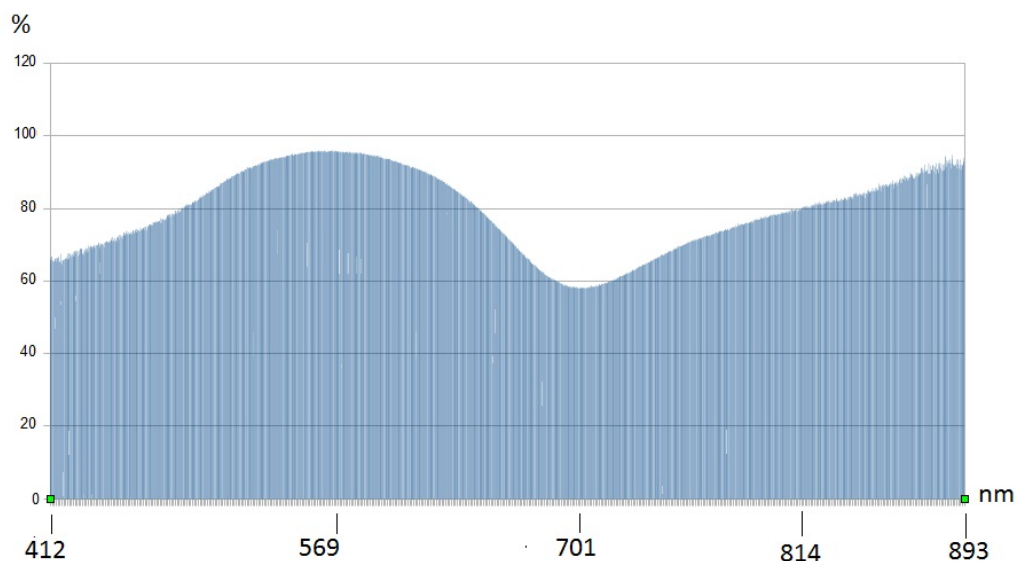


Figure 4.5: Plot of reflectance of *p* polarized light in percent vs wavelength in nm. The plot was recorded as described in section 3.1.9 The flow chambers contained water. The flowcell from the SR7000DC was used.

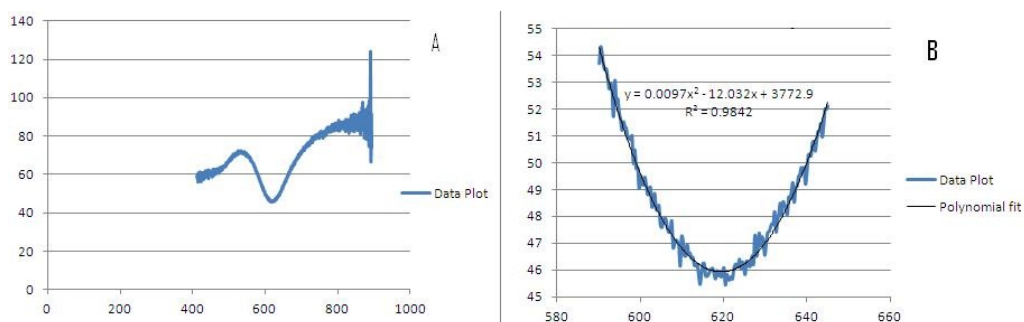


Figure 4.6: (A) Plot of reflectance of *p* polarized light in percent vs wavelength in nm. The plot was recorded as described in section 3.1.9 The flow chambers contained water. The custom made flowcell was used. (B) Zoom of the SPR dip with a second order polynomial fit

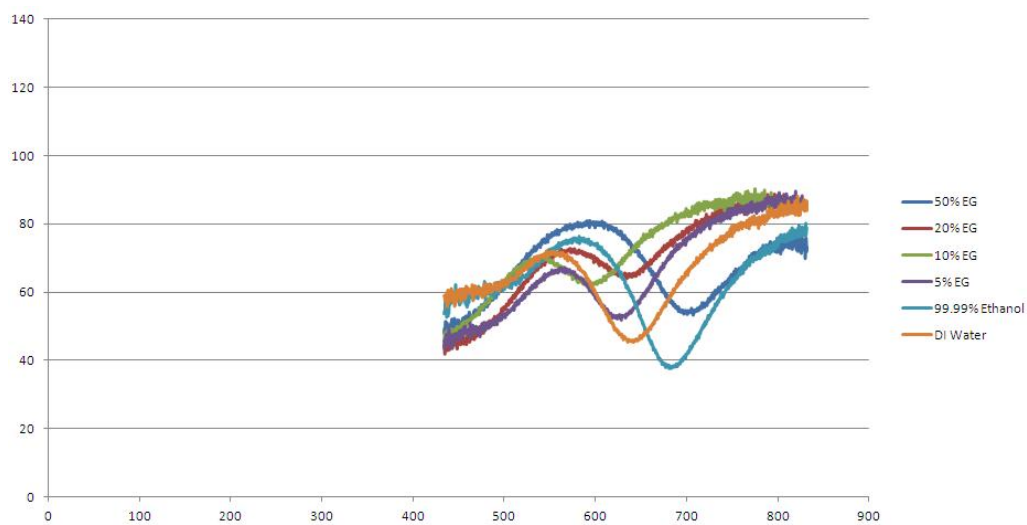


Figure 4.7: (A) Plot of reflectance of *p* polarized light in percent vs wavelength in nm. The plot was recorded as described in section 3.1.9 The flow chambers contained water. The custom made flowcell was used. (B) Zoom of the SPR dip with a second order polynomial fit

## 5.1 Discussion

### IL4 Binding Assay

Varying concentrations of IL4 was injected to bind to biotinylated DNA immobilized on a hydrogel, results can be seen in figure 4.1. They showed the expected response versus concentration correlation. The obtained curves follow the 1:1 model to some extent, but there are significant deviations, particularly in the  $2\mu M$  injection. In an attempt to avoid bubbles in the system, DI water was injected into the injection loop prior to injection of IL4 into the injection loop. This probably resulted in a less defined concentration profile. This could explain the poor fitting.

Kinetic values of  $k_a = 3.615$ ,  $k_d = 8.756 * 10^{-3}$ ,  $R_{max} = 3.193 * 10^5$  and  $K_d = 2.42228mM$  were obtained with residual standard deviations 13.636, 7.937 and 4.392 for  $2\mu M$ ,  $1\mu M$  and  $0.2\mu M$  respectively. The kinetic constants of IL4 were determined by Kasper R. Jensen to be  $k_a = 432$ ,  $k_d = 2 * 10^{-5}$  and  $K_d = 60mM$  Res sd = 6.379 for  $7.5\mu M$ . This was determined from a single injection and may not be reproducible, but as the standard deviation in the  $7.5\mu M$  injection is lower than that of  $1\mu M$  obtained in this report, it is probably more reliable. Hsu et. al. [19] reported konstants for indolicidin:  $k_a = 4770M^{-1}s^{-1}$ ,  $k_d = 0.19s^{-1}$  and  $K_d = 39.8\mu M$ , their  $k_a$  being 3 orders of magnitude higer and their  $k_d$  being 2 orders of magnitude higher.

### IL8 Binding Assay

IL4 binding assays were performed on a SPR Sensorchip HC 200m with biotinylated DNA immobilized. The curves behave as expected in terms of response versus concentration with the exception of  $1\mu M$  and  $0.5\mu M$  that are on top of each other. All concentrations except  $2\mu M$  seem to have dissociated completely after approximately 5 minutes.

The general response level is lower than that of IL4 and as a consequence the noise appears to be higher. This was confirme not to be the case by visual inspection of a zoomed version of figure 4.1 (result not shown).

The fit is better for the asociation phase than for the disociation phase and the disociation phase appears to be generally affected by artifacts. The curve from the asociation phase is generally followed well by the curve fit to the 1:1 binding model where the disociation phase shows significant deviation. In order to reach a steady state response flowrate was decreased to  $20\mu M$  and injection time was set to up to 50 minutes steady state was not observed and due to the low flowrate the noise level was significantly higher and artifact stemming from different concentration profiles were even more pronounced. Therefore these results have been omitted.

### Parallel Vs Serial Chamber Connection

A typical sensorgram of an injection of  $5\mu M$  IL4 is shown in figure 4.3 and it shows the problems asociated with serial injections of samples. In this case the problem is more pronounced at the start of the injection. This results in poor curve fittings as the fitting with either use a curve starting below 0 or alternatively one may move the injection time to the time when the response reaches 0 again after dropping below resulting in a fit to a more steep asociation phase than is actually the case.

A possible solution to the problem of different concentration profiles in the respective chamber would be to connect the chamber in parallel and attempt to keep the distance from the split of the flows to the respective chambers equal. This should also solve the problem of concentration smearing by mixing as the number of tube diameter changes would be the same which in theory should mean that the mixing should also be the same. Cutting the tubing may lead to lengths that aren't exactly the same and the chambers are hand drilled and may therefore vary slightly in size. This may result in different flowrates through the respective chambers. If the flowrates through the chambers is not the same it will result in a problem similar to the non identical smearing in serial flow in that the sample will enter one chamber more slowly than the other creating unnecessary artifacts at the beginning and the end of each injection.

To solve this potential issue one may alter the flow resistance of the tubing leading to and from one chamber in order for it to correspond better with that of the other. This may be done by cutting off a length of tubing leading to or from either chamber. While the tubing leading from the flowsplit to the chambers is relatively short, the tubing leading from the chamber to the waste receptacle is not and it may be used more easily.

The flow resistance of each chamber and the associated tubings can be determined from

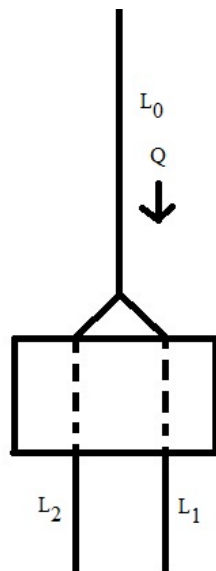


Figure 5.1: Schematic representation of parallel injection setup

the total flowrate,  $Q$ , and the ratio between the time it takes from the injection valve is turned till the sample reaches the two chambers respectively. Figure 5.1 shows the setup used. The Hagen- poiseuille law states [33]

$$\Delta p = R_{hyd}Q \quad (5.1)$$

Which for a circular tube is [35]:

$$\Delta p = \frac{8\eta LQ}{\pi a^4} \quad (5.2)$$

where  $L$  is the length of the tube,  $\eta$  is the dynamic viscosity and  $a$  is the radius of the circular cross section.

Applying equation 5.1 to the setup yields two equations; one for each chamber:

$$\Delta p = R_{hyd1}Q_1 \quad (5.3)$$

$$\Delta p = R_{hyd2}Q_2 \quad (5.4)$$

Combined these show the relationship between the flow rates and hydraulic resistances.

$$\frac{R_{hyd2}}{R_{hyd1}} = \frac{Q_1}{Q_2} \quad (5.5)$$

This also shows that the relationship between the separate flowrates remains constant even as the overall flowrate of the system changes.

The distance between the splitting of the flow to the the respective chambers is the same as is the diameter of the tube used. Therefore the time taken for the sample to reach the chamber is calculated in the same way:

$$t_1 = \frac{l}{v_1} \quad (5.6)$$

$$t_2 = \frac{l}{v_2} \quad (5.7)$$

With  $l$  being the length of the tube and  $v$  being the speed of the fluid given by:

$$v_1 = \frac{Q_1}{A} \quad (5.8)$$

$$v_2 = \frac{Q_2}{A} \quad (5.9)$$

Inserting into the expression for  $t_1$  and  $t_2$  it can be seen that the relationship between the  $t_1$  and  $t_2$  is the same as between  $R_{hyd1}$  and  $R_{hyd2}$

$$\frac{t_2}{t_1} = \frac{lQ_1A}{lQ_2A} = \frac{Q_1}{Q_2} = \frac{R_{hyd2}}{R_{hyd1}} \quad (5.10)$$

It is not feasible to determine the exact resistance of each chamber and the associated tubing it is possible to calculate the resistance of the waste tubes. It is then assumed that the waste tubes are responsible for all of the resistance in the system after the split. While it is not strictly true that it is responsible for all resistance, it is true that the waste tube is thinner and far longer than the tubing immediately after the split making it responsible for the majority of the resistance. The ratio of the flowrate in the left chamber to the flowrate in the right chamber is then determined via SPR by looking at the difference between the time it takes for the sample to reach each individual chamber. This ratio reveals the ratio between the resistances and by calculating the resistance of the left waste tube the assumed resistance of the right tube can then be calculated by multiplying the ratio with the calculated resistance of the left tube.

From this it can be determined how much of either the left or the right tube must be cut off in order to achieve the same resistance and thus flow rate in both chambers. The length of tubing calculated in this way will be smaller than the actual length required leading to an error on the side of caution.

Injections of indolicidin seen in figure 4.4 show the consequences of the parallel injection setup: The artifacts are far worse than in the serial connection setup. This is strange since the flows were at least fairly close to reaching the chambers at the same time. This must mean that Taylor Dispersion is not sufficient to describe the problem regarding the

difference in concentration profiles. Taylor Dispersion does not take turns and bends into account. The tubes leading from the point where the flow is split are bent quite a lot and it could be that one of them is bent slightly more than the other causing different flow in that tube. This is also the case with the hand drilled flowchambers, there may be small differences between the chambers causing the difference in concentration profile.

Injections of ethylene glycol were performed in order to determine how to create uniform flows in the two chambers when connected in parallel. The flowrate was not entirely stable which further complicates the configuration. The flowrate changes from time to time and not necessarily so the ratio of times from injection till signal remains the same. If this relationship changes during an injection, one injection will become slightly longer than other making it impossible to align the obtained curves properly. A possible solution to this could be if the flow was not split until right after it entered the flow cell. If this was done from the factory with completely identical internal channels in the flow cell, the flows would also be completely identical. In theory this would make the concentration profiles identical and thus the buffer change responses on the sensorgram would also be identical.

### **Immobilization of Thiolated DNA and Binding of Indolicidin to DNA**

Thiolated DNA was immobilized on a bare gold sensor chip as described in section 3.1.4. The signal changes obtained during the binding of thiolated DNA were fairly small. Larger than the change normally caused by a drifting baseline, but during the injections the signal was disturbed either by bubbles in the system causing a -1 response in the sensorgram, or by a sudden drop in response level with no apparent cause. This makes it very hard to determine if any binding took place during the injection.

This will have to be determined by examining the binding curves of indolicidin as indolicidin is known to bind to DNA [19]. Binding in the reaction chamber could also be due to binding of indolicidin to the mercapto layer. In order for this to be the case the layer would have to be more dense in the reaction chamber than in the reference chamber. This could happen if the binding in the reaction chamber reduced the amount of mercaptohexanol available for binding in the reference chamber. However it has been shown that mercaptoundecanoic acid forms a layer very quickly [36] and it seems likely that mercaptohexanol also behaves like this. Therefore it is unlikely that any difference between reaction chamber and reference chamber is the result of binding to the mercaptohexanol layer.

Binding of indolicidin to DNA was observed and the response versus concentration behaved as expected. This further supports binding of thiolated DNA to the gold surface.

The best fit to the data from the parallel injections of indolicidin was that of a model that takes mass transport into account. This is strange since it did not appear to fit any injections on the hydrogel chip which is known for its higher binding capacity [23]. A higher concentration of DNA would make mass transport limitation more likely. So it is unlikely that the mass transport model fits better because of actual mass transport. A possible explanation could be binding to the mercaptohexanol layer: The mercaptohexanol layer has a negative charge and indolicidin is positively charged, meaning there is an electrostatic attraction. Another possibility is that the mercaptohexanol layer acts as pseudo membrane; it has a hydrophilic OH group in contact with the solution and it has a hydrophobic carbon chain attached to it. Thiol self assembled monolayers are densely packed [36] and thus it should not be possible for indolicidin to penetrate the layer to place its hydrophobic residues in close proximity with the carbon chain of mercaptohexanol. However Indolicidin is known to bind to bacterial membranes by inserting itself in a wedge shape. It is possible that it may be able to insert itself in a similar way in the densely packed monolayer.

Kinetic values obtained from parallel injections of indolicidin are:  $k_m = 55272.5$   $k_a = 824 * 10^7$ ,  $k_d = 775.7$   $K_d = 9.41478 \mu M$ . R max values of 2930.2, 4023.5, 3814.3 and 1916.1 for  $2 \mu M, 0.2 \mu M, 0.5 \mu M$  and  $1 \mu M$  respectively and Residual standard deviations of 3.456, 2.542, 2.691 and 2.665 for  $2 \mu M, 0.2 \mu M, 0.5 \mu M$  and  $1 \mu M$  respectively. Hsu et. al reported values of  $k_a = 4770 M^{-1} s^{-1}$ ,  $k_d = 0.19 s^{-1}$  and  $K_d = 39.8 \mu M$  [19].  $k_a$  obtained in this report are 4 orders of magnitude higher than  $k_a$  obtained by Hsu. Considering the large amount of very significant artifacts the values for indolicidin obtained in this report are complete unreliable.

### White Light SPR

At first the flow cell from the SR7000DC was used and it was filled with water. The resonance wavelength was around 700 which was unexpected as calculations had determined that the resonance wavelength should be around 600. This was thought to be because the portion of the chip in contact with the contents of the flowcell is very small compared to the size of the chip and for this reason a new flowcell was designed. The new flowcell contains only one chamber which takes up the majority of the chip.

With the new flow cell the resonance wavelength was found to be much closer to the expected value, which signifies that the measured resonance wavelength of around 700nm was made with rubber and air as dielectrics and only to a small extent the water in in the flowcell.

Reflectance curves *p – polarized/s – polarized* were obtained with water, ethanol, 5%, 10%, 20% and 50% ethylene glycol in the flow new cell. The minimum of reflectance was determined to be at 619.74nm, 652.04nm, 605.41nm, 605,43nm, 629.18nm and 700nm. respectively.

The SPR feature is observed to change as the gold surface comes into contact with liquids of different refractive indexes, thus reflectance curves obtained with p-polarized light show the characteristic SPR dip. The position of this dip depends on the refractive index of the solution in the fluidic chamber.

There is an oddity in that pure water shows a higher resonance wavelength than both 5% and 10% ethylene glycol. This is probably an error in the resonance wavelength for water. It is possible that liquid in the new flowcell is not entirely pushed out when a new injection is done. This was observed to be the case for purging the flowcell with an air injection, the SPR dip for water was still observed though the dip was more shallow. The higher resonance wavelength could in this fashion be the result of an old injection of ethanol.

# Conclusion

---

## 6.1 Conclusion

Binding of indolicidin, IL4 and IL8 to DNA was experimentally investigated using a commercial SPR spectrometer. Two methods of DNA immobilization were tested: thiolated DNA immobilized on bare gold surface and biotinylated DNA immobilized to polycarboxylate hydrogel via covalently bound streptavidin. DNA was found to bind in both cases. The conducted experiments demonstrated indolicidin and IL4 binding to DNA while no binding of IL8 to DNA was observed. However, it was not possible to determine reliable kinetics values due to the experimental artefacts.

SPR experiments involving binding of indolicidin and its analogues are extremely challenging due to significant non-specific binding and, possibly, tendency of the peptide to aggregate. In an attempt to improve referencing in SPR, the parallel arrangement of reference and measurement cells was tested. Under an assumption that identical parallel flow through reference and measurements cell will create identical environment for non-specific binding, a set of indolicidin-DNA binding experiments was performed with parallel arrangement of the cells. However, the parallel connection with external tubing did not show any benefits compared to the serial connection in terms of artefacts in the treated binding curves. It can be suggested that due to strong flow bending at the inlet and outlet of the chambers, a small deviations in mechanical design of the chambers can produce significant spread in the concentration profiles even at the same flow through the cells.

White-light SPR setup was assembled. This type of SPR measurement can be beneficial for studies involving plasmons localized (LP) on nanoparticles or nanostructures as the position of SPR dip can be continuously tuned to the chosen part of the spectrum. The measurements showed a characteristic SPR dip for p-polarized light the position of which depended on the refractive index of the solution inside the fluidic chamber. With the current experimental setup and the gold chips used we could position the dip down to approximately 600nm for aqueous solutions.

# Bibliography

- [1] Charles Marwick. Animal feed antibiotic use raises drug resistance fear. *JAMA: The Journal of the American Medical Association*, 282(2):120–122, 1999.
- [2] Sherwood L. Gorbach. Antimicrobial use in animal feed - time to stop. *New England Journal of Medicine*, 345(16):1202–1203, 2001.
- [3] Wegener HC, Aarestrup FM, Jensen LB, and Hammerum AM. Use of antimicrobial growth promoters in food animals and enterococcus faecium resistance to therapeutic antimicrobial drugs in europe. *Emerging Infectious Diseases*, 5:329–335, 1999.
- [4] Kim A Brogden, Mark Ackermann, Paul B McCray Jr., and Brian F Tack. Antimicrobial peptides in animals and their role in host defences. *International Journal of Antimicrobial Agents*, 22(5):465 – 478, 2003.
- [5] Gaynes R. and Monnet D. The contribution of antibiotic use on the frequency of antibiotic resistance in hospitals. *Ciba Foundation Symposium*, 207:47–56, 1997.
- [6] David I. Chan, Elmar J. Prenner, and Hans J. Vogel. Tryptophan- and arginine-rich antimicrobial peptides: Structures and mechanisms of action. *Biochimica et Biophysica Acta (BBA) - Biomembranes*, 1758(9):1184 – 1202, 2006. Membrane Biophysics of Antimicrobial Peptides.
- [7] Jeanette H. Andersen, Haavard Jenssen, Kjersti Sandvik, and Tore J. Gutteberg. Antihsv activity of lactoferrin and lactoferricin is dependent on the presence of heparan sulphate at the cell surface. *Journal of Medical Virology*, 74(2):262–271, 2004.
- [8] Anthony J. De Lucca and Thomas J. Walsh. Antifungal peptides: Novel therapeutic compounds against emerging pathogens. *Antimicrob. Agents Chemother.*, 43(1):1–11, 1999.
- [9] N. Papo and Y. Shai. Host defense peptides as new weapons in cancer treatment. *Cellular and Molecular Life Sciences*, 62:784–790, 2005. 10.1007/s00018-005-4560-2.
- [10] Z Oren, J C Lerman, G H Gudmundsson, B Agerberth, and Y Shai. Structure and organization of the human antimicrobial peptide ll-37 in phospholipid membranes: relevance to the molecular basis for its non-cell-selective activity. *Biochem. J.*, 341(3):501–513, 1999.
- [11] Kim A. Brogden. Antimicrobial peptides: Pore formers or metabolic inhibitors in bacteria? *Nature*, 3:338–350, 2005.
- [12] Michael R. Yeaman and Nannette Y. Yount. Mechanisms of antimicrobial peptide action and resistance. *Pharmacological Reviews*, 55(1):27–55, 2003.

## BIBLIOGRAPHY

---

- [13] Alexey S. Ladokhin, Michael E. Selsted, and Stephen H. White\*. Bilayer interactions of indolicidin, a small antimicrobial peptide rich in tryptophan, proline, and basic amino acids. *Biophysical Journal*, 72:794–805, 1997.
- [14] C. Subbalakshmi, E. Bikshapathy, N. Sitaram, and R. Nagaraj. Antibacterial and hemolytic activities of single tryptophan analogs of indolicidin. *Biochemical and Biophysical Research Communications*, 274(3):714 – 716, 2000.
- [15] Aaron P. Podorieszach and Heidi E. K. Huttunen-Hennelly. The effects of tryptophan and hydrophobicity on the structure and bioactivity of novel indolicidin derivatives with promising pharmaceutical potential. *Org. Biomol. Chem.*, 8:1679–1687, 2010.
- [16] Jochen Wiesner and Andreas Vilcinskas. Antimicrobial peptides: the ancient arm of the human immune system. *Virulence*, 1(5):440–464, 2010.
- [17] Ziv Oren and Yechiel Shai. Mode of action of linear amphipathic alpha-helical antimicrobial peptides. *Peptide Science*, 47(6):451–463, 1998.
- [18] Sung-Min Kim, Joung-Min Kim, Bishnu Prasad Joshi, Hyeongjin Cho, and Keun-Hyeung Lee. Indolicidin-derived antimicrobial peptide analogs with greater bacterial selectivity and requirements for antibacterial and hemolytic activities. *Biochimica et Biophysica Acta (BBA) - Proteins and amp; Proteomics*, 1794(2):185 – 192, 2009.
- [19] Chun-Hua Hsu, Chinpan Chen, Maou-Lin Jou, Alan Yueh-Luen Lee, Yu-Ching Lin, Yi-Ping Yu, Wei-Ting Huang, and Shih-Hsiung Wu. Structural and dna-binding studies on the bovine antimicrobial peptide, indolicidin: evidence for multiple conformations involved in binding to membranes and dna. *Nucleic Acids Research*, 33(13):4053–4064.
- [20] J. M. Pitarke, V. M. Silkin, E. V. Chulkov, and P. M. Echenique. Theory of surface plasmons and surface-plasmon polaritons. *REPORTS ON PROGRESS IN PHYSICS*, 70(1):1–87, 2007.
- [21] Miles V. Klein and Thomas E. Furtak. *Optics*. John Wiley and sons, 1986.
- [22] Yu F. Surface plasmon fluorescence spectroscopy and surface plasmon diffraction in biomolecular interaction studies. 2004.
- [23] Jiri Homola. *Surface Plasmon Resonance Based Sensors*. Springer, 2006.
- [24] Fariyal A. Tanious, William Laine, Paul Peixoto, Christian Bailly, Kristie D. Goodwin, Mark A. Lewis, Eric C. Long, Millie M. Georgiadis, Richard R. Tidwell, and W. David Wilson. Unusually strong binding to the dna minor groove by a highly twisted benzimidazole diphenylether: Induced fit and bound water. *Biochemistry*, 46(23):6944–6956, 2007. PMID: 17506529.
- [25] Olli H. Laitinen, Henri R. Nordlund, Vesa P. Hytonen, and Markku S. Kulomaa. Brave new (strept)avidins in biotechnology. *Trends in Biotechnology*, 25(6):269 – 277, 2007.
- [26] Ken A. Dil and Sarina Bromberg. *Molecular Driving Forces*. Garland Science, 2003.
- [27] *BIAtechnology Handbook*. Biacore AB, 1998.
- [28] Peter Schuck and Allen P. Minton. Kinetic analysis of biosensor data: elementary tests for self-consistency. *Trends in Biochemical Sciences*, 21(12):458 – 460, 1996.

- [29] Daniel J. O'Shannessy and Donald J. Winzor. Interpretation of deviations from pseudo-first-order kinetic behavior in the characterization of ligand binding by biosensor technology. *Analytical Biochemistry*, 236(2):275 – 283, 1996.
- [30] D.J. Oshannessy, M. Brighamurke, K.K. Soneson, P. Hensley, and I. Brooks. Determination of rate and equilibrium binding constants for macromolecular interactions using surface plasmon resonance: Use of nonlinear least squares analysis methods. *Analytical Biochemistry*, 212(2):457 – 468, 1993.
- [31] Peter Schuck and Allen P. Minton. Analysis of mass transport-limited binding kinetics in evanescent wave biosensors. *Analytical Biochemistry*, 240(2):262 – 272, 1996.
- [32] Rebecca L. Rich and David G. Myszka. Grading the commercial optical biosensor literature-class of 2008: The mighty binders. *Journal of Molecular Recognition*, 23(1):1–64, 2010.
- [33] Henrik Bruus. *Theoretical Microfluidics*. Oxford, 2008.
- [34] Mikhail Polyanskiy. Refractive index database. <http://refractiveindex.info/>, 2008-2011.
- [35] Bruce R. Munson, Donald F. Young, and Theoore H. Okiishi. *Fundamentals of Fluid Mechanics*. John Wiley and sons, 2005.
- [36] Flavio S. Damos, Rita C. S. Luz, and Lauro T. Kubota. Determination of thickness, dielectric constant of thiol films, and kinetics of adsorption using surface plasmon resonance. *Langmuir*, 21(2):602–609, 2005.